Noxious effects of cell surface display glutamate sensors on plant growth and development

Vanessa Castro-Rodríguez[1], Thomas J. Kleist[1], Nicoline M. Gappel[1], Sakiko Okumoto[2], Mackenzie Machado[3], Tom Denyer[4], Marja C. P. Timmermans[4], Wolf B. Frommer[1,5,*] & Michael M. Wudick[1]

Affiliations:

[1] Institute for Molecular Physiology, Heinrich Heine Universität Düsseldorf, Germany

[2] Department of Soil and Crop Science, Texas A&M, College Station, TX, USA

[3] Dep. Plant Biology, Carnegie Institution for Science, Stanford, CA, USA

[4] Center for Plant Molecular Biology, University of Tübingen, Auf der Morgenstelle 32, 72076 Tübingen, Germany

[5] Institute of Transformative Bio-Molecules (WPI-ITbM), Nagoya University, Chikusa, Nagoya 464-8601, Japan

*Correspondence: frommew@hhu.de

SUMMARY

Plants use electrical and chemical signals for systemic communication. Herbivory, for instance, appears to trigger local apoplasmic glutamate accumulation, systemic electrical signals and calcium waves that travel to report insect damage to neighboring leaves and initiate defense. To monitor extra- and intracellular glutamate concentrations in plants, we generated lines expressing genetically encoded fluorescent glutamate sensors. In contrast to cytosolically localized sensors, extracellularly displayed variants inhibited plant growth and proper development. Phenotypic analyses of high-affinity display sensor lines revealed that root meristem development, particularly the quiescent center (QC), the number of lateral roots, vegetative growth and flower architecture were affected. Notably, the severity of the phenotypes was proportional to the affinity of the displayed glutamate sensors, intimating that their ability to bind extracellular glutamate caused the observed defects. Congruously, root growth defects were suppressed by supplementing culture media with low levels of glutamate. Overall, our data indicate sensor noxiousness was dependent on its membrane-tethering and likely caused by sequestration of extracellular glutamate, specifically at the cell surface, thereby either disrupting the supply of glutamate to meristematic cells and/or by impairing local glutamatergic signaling during development.

KEYWORDS

Arabidopsis thaliana, glutamate, root meristem, sensor

INTRODUCTION

As a building block of proteins and central player in metabolism, glutamate is an essential amino acid for all known forms of life. In addition, many organisms also utilize L-glutamate as a signaling molecule. Glutamatergic signaling has been most intensively studied in the context of the animal central nervous system, where it serves as an excitatory neurotransmitter through activation of metabotropic and ionotropic glutamate receptors. In plants, glutamate is essential for the assimilation of nitrogen and for amino acid transamination (Forde and Lea, 2007). Low amounts of externally supplied glutamate are known to affect root architecture by impairing primary root growth while favoring the development of secondary roots (Walch-Liu et al., 2006). Various lines of evidence implicate glutamate itself as a signaling molecule also in plants. This hypothesis is supported by the finding that mutants in *GLUTAMATE RECEPTOR-LIKE* (*GLR*) ion channel genes, proteins for which glutamate can act as an agonist, show altered wound responses as they are impaired in the propagation of wound-induced leaf variation potentials (electrical signals characterized by transient depolarization and delayed repolarization (Mousavi et al., 2013; Nguyen et al., 2018). Notably, it was shown that external application of glutamate to leaves elicits long-distance, calcium-based plant defense signaling responses (Toyota et al., 2018).

Genetically encoded biosensors that rely on the change in fluorescence resonance energy transfer (FRET) efficiency of two fluorescent proteins (FPs) have been engineered and used to dynamically report levels of several metabolites and signaling molecules in living cells (Frommer et al., 2009; Okumoto et al., 2012). By sandwiching a bacterial periplasmic binding protein (YbeJ) between enhanced cyan FP (ECFP) and Venus, a yellow FP (YFP) variant (Okumoto et al., 2005), engineered one of the first FRET-based fluorescent indicator proteins for glutamate (FLIPE). Subsequent systematic modification of this first-generation glutamate sensor yielded a series of optimized sensors with varying ligand affinities and dynamic ranges (Deuschle et al., 2005), however, these variants could not be used in neuronal cells since they did not traffic efficiently to the cell surface (Okumoto unpublished). Subsequently, intensiometric single-fluorophore sensors called iGluSnFRs have also been engineered by insertion of a circularly permutated green FP (cpGFP) into YbeJ (Marvin et al., 2013). Toyota et al., (2018) successfully targeted these sensors to the cell wall space to estimate glutamate concentrations after wounding of Arabidopsis leaves (Toyota et al., 2018). Because cpGFP-based sensors are particularly sensitive to pH changes the use of ratiometric FRET-based sensors is often advantageous for *in vivo* imaging (Barnett et al., 2017). We therefore deployed a suite of FLIPE variants spanning a wide range of affinities to monitor changes in extra- and intracellular levels of glutamate in Arabidopsis.

Plants expressing cytosolic versions of the sensor showed wild type-like growth phenotypes. Unexpectedly, when the sensors were plasma membrane-anchored and displayed at the cell surface, plants were severely stunted and showed defects in root and flower development. The severity of the phenotype was dependent on the affinity of the sensor and symptoms could be ameliorated by supplementation with glutamate, consistent with a model wherein surface-expressed sensors interfere with the glutamate availability close to the plasma membrane and thereby disrupt growth and development.

RESULTS

Expression of extracellularly displayed FLIPEs causes stunting and lethality

To generate plants for quantitative imaging of glutamate dynamics, a suite of FLIPE affinity variants was introduced into Arabidopsis and either produced in the cytosol (FLIPE^{cyt}) or tethered to the extracellular face of the plasma membrane, which we refer to here as 'display' sensor (FLIPE^{display}). FLIPE^{display} and FLIPE^{cyt} cassettes were constructed by sandwiching the *E. coli* periplasmic glutamate binding protein YbeJ, between two spectral variants of the green fluorescent protein (Fig. 1). Cell surface display was achieved by fusion of an ER targeting sequence to the N-terminus of the chimera and the mammalian PDGF receptor transmembrane spanning domain to its C-terminus. The sensors were expressed under control of the ubiquitous CaMV 35S promoter in *rdr6-11* silencing mutants. Transformants (T_1) showing homogeneous fluorescence were identified and used for further experiments (Fig. S1A).

To test whether the mammalian targeting sequences are functional and effective in targeting the sensor to the cell surface in Arabidopsis, confocal microscopy was used to localize Venus fluorescence in transgenic plants expressing FLIPE variants. While FLIPE^{display} sensors were detected at the plasma membrane, FLIPE^{cyt} sensors localized to the cytosol (Fig. 2A-F). The presence of the display sensors at the cell surface was assessed by preincubation with a protein synthesis inhibitor (cycloheximide, CHX) followed by proteinase K digestion in tobacco leaf protoplasts expressing a cytosolic, high-affinity sensor ($K_d \approx 600$ nM, FLIPE-600n^{cyt}) or a display sensor variant ($K_d \approx 1$ mM, FLIPE-1m^{display}), respectively. The fluorescence of protoplasts expressing the FLIPE-600n^{cyt} construct was not altered over the course of the experiment regardless of the treatment. However, a decrease in fluorescence of proteinase K-treated FLIPE-1m^{display}-expressing protoplasts was observed, consistent with the predicted sensor topology where the ligand-binding domain of YbeJ faces the apoplasmic space (Fig. 2D-E, Fig. S2). Perfusion of roots of lines expressing FLIPE-10µ^{display} with glutamate led to concentration-dependent changes in fluorescence ratio with a $K_{0.5}$ in the range of 10µM, consistent with the surface exposure of the sensors (Fig. S3). By contrast, we did not observe glutamate-induced responses in lines expressing the cytosolic sensors (data not shown). The ability to detect responses depends critically on the relative activity of plasma membrane transport, metabolism and compartmentation, thus these data indicate that uptake rates are too low to be detected with this sensor (Okumoto et al., 2008).

Plants expressing FLIPE^{cyt} variants were phenotypically indistinguishable from *rdr6-11* controls (Fig. 3A) and, accordingly, had similarly sized rosettes when grown in soil for six weeks (Fig. 3B). By contrast, plants expressing high-affinity FLIPE^{display} variants (600n^{display}, 10µ^{display}) were severely dwarfed, did not show substantial growth beyond week 3 (Fig S1B), and their leaves covered only about 20% of the rosette area of FLIPE^{cyt} and *rdr6-11* control plants ($n \geq 12$ plants) (Fig. 3A, B).

Our observations led us to posit that growth inhibition was caused by the noxiousness of the high affinity sensors when displayed by anchoring to the surface of the plasma membrane. We therefore tested for a possible correlation between the severity of growth defects and the affinity of the sensors for glutamate. To avoid possible additive detrimental effects of sensor noxiousness and stress caused by antibiotic selection, identification of primary transformants was solely based on Venus fluorescence. Fluorescent seedlings for all sensor variants were transferred to soil and systematically assessed for viability (Table 1). Nano- to micromolar affinity FLIPE^{display} variants (600 nM, 10 µM, 100 µM) reproducibly (n = 50-100 plants) were dwarfed. Moreover, plants expressing FLIPE-100µ^{display}, FLIPE-1m^{display}, as well as the cytosolic versions, were the only transgenic lines that reached the reproductive stage and generated seeds, albeit with different frequencies for display (9-32%) and cytosolic versions (99%) (Table 1). To further explore the dependence of noxiousness on the sensor affinity, sensor mutants with intermediate affinities (FLIPE-40µ^{display}, FLIPE-250µ^{display}, and FLIPE-500µ^{display}; Fig. 1, Fig. S4) were generated and

analyzed. To evaluate if the surface display rather than apoplasmic expression of the sensor was a prerequisite for its noxiousness, an additional apoplasm-targeted FLIPE-600n variant, which carried the ER targeting sequence but lacked the PDGFR transmembrane domain, was generated and localized in the cell wall space (FLIPE-600n^{apo}; Fig. 1, Fig. 2C, F). Recently, a similar cpGFP-based intensiometric glutamate sensor (iGluSnFR) was successfully employed to monitor glutamate concentration in the extracellular space in response to wounding (Toyota et al., 2018). In line with our observations, the authors did not report any noxious effects of the sensor. Noxiousness seems to be due to surface display, which is thought to specifically affect local glutamate levels at the membrane surface.

Phenotypic classification of the size of ≥ 6-weeks-old, soil grown transgenic plants into "dwarf" (< 5 cm), "intermediate" (≥ 5 cm, ≤ 15 cm) and "regular" (> 15 cm) revealed that the majority of plants expressing display sensors was dwarfed, plants expressing the FLIPE-600n^{display} sensor being most affected (95%; Fig. 3C). Consistent with an affinity-dependency of the phenotype, lower affinity mutants (250µ, 500µ) displayed more "intermediate" (up to 34%) or "regular" (up to 15%) growth phenotypes (Fig. 3C). Contrarily, the majority of FLIPE-600n^{apo}-expressing plants showed wild type-like growth (87%), indicating that tethering to the extracellular face of the plasma membrane, was crucial for its noxiousness. Specifically, we hypothesized that the extracellular display of high-affinity glutamate-binding FLIPEs may perturb glutamate availability in the apoplasm.

Developmental defects in FLIPE^{display} lines

A phenotypic analysis of FLIPE^{display}-expressing plants was performed to determine if the noxious effect of the FLIPE^{display} sensors impacted other aspects of plant development. Flowers from control *rdr6-11* and FLIPE^{cyt}-expressing plants were anatomically indistinguishable. Flower morphology was significantly different between FLIPE^{display} and FLIPE^{cyt} versions (Fig. 4). Typically, flowers from dwarfed FLIPE^{display} plants were characterized by deformed or missing petals and appeared developmentally delayed, affecting reproductive efficiency of FLIPE^{display} plants (Fig. 4, Table 1). FLIPE^{display} lines tended to have shorter roots, an effect that correlated with sensor affinity to glutamate (*i.e.*, higher affinities for glutamate yielded plants with shorter primary roots). Since the extracellular glutamate concentration is known to impact mitotic activity in the root apical meristem (RAM, (Walch-Liu et al., 2006)), RAMs from select FLIPE lines were examined. The majority of roots stably expressing the high-affinity FLIPE-600n^{display} sensor was severely deformed, likely due to aberrant growth and irregular cell division (Fig. S5). Consequently, FLIPE-600n^{display}-expressing roots that did not allow us to correctly assign cell identities and tissue layers were excluded from further analyses. While plants expressing FLIPE-10µ^{display} and FLIPE-100µ^{display} sensors also showed defective cell division patterns in the root meristem, affecting the quiescent center (QC), columella and root cap cells, none of the roots were as severely affected as the roots expressing the FLIPE-600n^{display} sensor (Fig. 5A, B). After 3-5 days of growth, the columella of control seedlings typically consists of five tiers of cells, one or two of which represent stem cell tiers while the remaining tiers of differentiated cells are characterized by an accumulation of starch granules (Kiss et al., 1996). We observed similar cell patterns in RAMs of plants expressing FLIPE-600n^{cyt}, FLIPE-10µ^{cyt} as well as FLIPE-1m^{display} sensors and *rdr6-11* controls (Fig. 5A, B). By contrast, more than 80% of roots from FLIPE-600n^{display}-expressing plants apparently lacked the distal stem cell layer and displayed irregular columella cell division patterns (Fig. 5B, C). Although roots from plants expressing FLIPE-10µ^{display} and FLIPE-100µ^{display} constructs showed disorganized QC and columella cells, more than 50% of the mutants displayed at least one stem cell tier (Fig. 5C). This indicates that defects in the stem cell niche (affecting the overall number of cells) in plants expressing FLIPE^{display} constructs likely caused reduced root growth. As we also observed developmental defects in the vegetative tissue, it is possible that high-affinity FLIPE^{display} sensors also impact the development of the shoot meristem. Though not studied in detail here, together with

the observed alterations in flower morphology, this tentatively points to a broad role of glutamate in developmental processes.

Glutamate supplementation mitigates root growth defects in FLIPE^{display} lines

The affinity-dependent phenotypes of FLIPE^{display} lines indicate that noxiousness may be caused by disruption of extracellular glutamate levels. Presumably, extracellular display of FLIPE proteins reduces the levels of free glutamate in the apoplasm through competitive binding or 'buffering'. We therefore hypothesized that the growth defects could be suppressed by supplementing media with glutamate. Six-days-old seedlings expressing FLIPE^{display} or FLIPE^{cyt} constructs or untransformed controls were transferred from half-strength MS media to fresh media with different glutamate concentrations (Fig. 6). Exogenously supplied L-glutamate (eGlu) is known to impair primary root growth and to increase the number of secondary roots in control plants (Walch-Liu et al., 2006). Accordingly, while low concentrations of eGlu (0-25 µM) had little to no effect on the root length of *rdr6-11* control plants, higher eGlu concentrations (> 100 µM) resulted in shorter primary roots (Fig. 6). In contrast, root lengths of FLIPE-600n^{display}-expressing plants increased up to two-fold when grown on media with 25-1000 µM eGlu, thus at least partially suppressing the dwarf phenotype. Hence, even at eGlu concentrations that inhibited root growth *in rdr6-11* plants, FLIPE-600n^{display}-expressing plants showed increased primary root lengths compared to roots of plants grown in the absence of eGlu (Fig. 6A). While glutamate concentrations > 25 µM elicited a previously described increase in the number of lateral roots in *rdr6-11* control plants (Walch-Liu et al., 2006), FLIPE-600n^{display} plants did not show an altered lateral root number (Fig. 6B). Overall, eGlu treatment caused opposite effects in *rdr6-11* control and FLIPE-600n^{display}-expressing plants. The altered availability of extracellular glutamate could affect the supply of glutamate to meristematic cells and/or glutamate-mediated signaling processes in the plant, ultimately causing the observed phenotypes. To distinguish between these two hypotheses, we analyzed the cell type-specific accumulation of mRNAs associated with glutamate biosynthesis.

Transcripts of glutamate-associated genes are present in QC and surrounding cells

To profile glutamate-associated gene expression, single cell RNA sequence (scRNA-seq) data from Arabidopsis root tips of 6-day-old seedlings, clustered by cell type and developmental stage (Denyer et al., 2019) was analyzed. Plants are able to synthesize glutamate through different enzymatic pathways, *i.e.* involving genes coding for *GLUTAMINE-α-OXOGLUTARATE AMINOTRANSFERASE* (*GOGAT*), *GLUTAMINE SYNTHETASE* (*GS*) and *GLUTAMATE DEHYDROGENASE* (*GDH*) in the presence of a nitrogen source (Forde and Lea, 2007). Our analysis revealed that transcripts of three different *GS* isoforms (*GS1;1*, *GS1;3* and *GS2*), as well as of *GOGAT2*, *GDH1* and the ammonium transporter *AMT1.1* were indeed detected in the QC and/or in its surrounding cell layers (Fig. S6), consistent with the ability of these cells to synthesize glutamate on their own. While transcripts of genes for possible down-stream targets of glutamate, *i.e.* members of the *GLUTAMATE RECEPTOR-LIKE* (*GLR*) family, were lowly expressed and lacked a specific expression pattern, transcripts of a putative *LYSINE/HISTIDINE TRANSPORTER* gene (*LHT4*) were enriched in QC and surrounding cells (Fig. S6). Of note, close homologs of this transporter were previously shown to transport glutamate in rice (*Os*LHT1) and Arabidopsis (*At*LHT1) (Hirner et al., 2006; Wang et al., 2019). Taken together, transcriptomic data indicate that meristem cells of the root may be capable of ensuring adequate supply with glutamate by either synthesis from imported ammonium. This observation, together with the fact that only display sensors cause noxiousness, is consistent with an effect of sensor display-triggered scavenging of glutamate on glutamate signaling during plant development.

DISCUSSION

With the initial intent to monitor glutamate levels *in planta*, Arabidopsis lines stably expressing a suite of FRET-based fluorescent indicator proteins for glutamate (FLIPE) were generated. Unexpectedly, plants expressing high-affinity FLIPE display variants were severely dwarfed and showed reduced fertility. The severity of the phenotype correlated with the affinity of the sensors for glutamate (*i.e.*, high-affinity variants caused the most dramatic phenotypes). Characterization of the YbeJ binding domain revealed that it binds glutamate an order of magnitude higher affinity than aspartate, and has substantially lower affinities for glutamine and asparagine (Okumoto et al., 2005; Willis and Furlong, 1975). We therefore hypothesized that the phenotypes were caused by depletion of the glutamate pool at the cell surface due to the glutamate-binding activity of FLIPE constructs. Correspondingly, the same high-affinity construct (FLIPE-600n) was only noxious when anchored at the plasma membrane facing the apoplasm, while neither cytosolically, nor apoplasmically secreted variants produced noxious effects. Consistent with the hypothesis of glutamate depletion, supplementation of the media with extracellular glutamate partially restored growth in plants expressing extracellularly displayed, membrane-anchored high-affinity sensors. Sensor noxiousness could either be due to glutamate starvation in particular cell types, *i.e.* in the root apical meristem, or the product of perturbed glutamatergic signaling. The observation that transcripts for several glutamate-related genes are present in root meristematic cells, appears at odds with the hypothesis that defects in glutamate nutrition cause FLIPE noxiousness. Moreover, sequestration of glutamate either in the cell wall space or the cytosol (in plants expressing sensors targeted to the apoplasm or cytosol, respectively) would be expected to interfere with metabolism as well. We thus cautiously hypothesize that FLIPE sensors interfere with glutamatergic signaling at the membrane surface, likely by local buffering of glutamate pools in the vicinity of GLRs, which may interfere with downstream signaling processes. Sequestration or buffering by transgenes has been described in plants, e.g. in the case of a genetically encoded cAMP-sponge (Sabetta et al., 2019), or a parvalbumin-derived calcium buffer (Huang et al., 2017).

For glutamate to function as a signal molecule, it needs to be kept at low resting levels in the extracellular space, particularly in the vicinity of glutamate receptors. In animals, this is achieved by the action of multiple sets of transporters in the cells that release glutamate, the cells that perceive the signal and the adjacent glial cells (Mahmoud et al., 2019). A main difference between plants and animals, however, is that the synaptic cleft is minute in volume, thus requiring only small amounts of glutamate to be released and subsequently taken up again for desensitization, while the apoplasmic space between plant cells is orders of magnitude larger, indicating the need for different mechanisms. Therefore, efficient glutamate uptake and redistribution mechanisms are particularly important in plants, which use glutamate as a major transport form of nitrogen. Indeed, while in plants, the concentration of most amino acids may change substantially during the diurnal cycle, glutamate in leaves appears to be homeostatic between 0.3 – 1.3 mM, depending on the species (Forde and Lea, 2007). Glutamate receptor-like proteins (GLRs) had previously been implicated in meristem maintenance, developmental regulation and glutamatergic signaling processes in roots (Li et al., 2006; Singh et al., 2016; Singh and Chang, 2017; Vincill et al., 2013). Similar to FLIPE^{display}-expressing plants, rice plants carrying mutations in *GLR3.1* displayed short roots with reduced QC cell numbers and an impaired cell division activity of the RAM (Li et al., 2006). Further evidence that glutamate-induced, GLR-mediated signaling is important for root development comes from the observation that glutamate receptor agonists negatively affected the primary root length and the number of secondary roots (Singh and Chang, 2017). The authors reported that, similar to the effects of glutamate resupply on FLIPE-expressing lines, exogenous application of glutamate was able to restore primary root growth as well as the number of lateral roots, further indicating that root development relies on glutamate signaling processes.

The noxious effects of FLIPE^{display} sensors render them unsuitable for glutamate imaging, for instance during wounding. Analysis of glutamate dynamics are thus best performed with apoplasmic glutamate sensors. To further improve sensor performance, Matryoshka-type indicators, along with affinity mutants to control for artifacts, should be employed, as they are ratiometric, have an increased dynamic range and are less affected by changes in pH (Ast et al., 2017).

In summary, our data indicate that the level of glutamate specifically at the cell surface is important for glutamatergic signaling, thus requiring tight control via transport processes. Moreover, our data may support a role of glutamate in the regulation of developmental processes, in particular in root, shoot and floral meristems.

Material and Methods

FLIPE constructs for plant transformation

FLIPE surface display constructs carrying tandemly fused murine Ig kappa-chain (IGK) signal peptides, the YbeJ coding sequence (also called GltI; NP_415188, amino acid residues 29 - 302), and the transmembrane domain of the platelet-derived growth factor receptor (PDGFR) were constructed as described previously (Okumoto et al., 2005). The YbeJ coding sequence was sandwiched between sequences encoding enhanced cyan fluorescent protein (ECFP) and Venus, a yellow FP. The resulting construct was excised using *BamH*I/*Xho*I, and subcloned into *BamH*I/*Sal*I sites of the plant expression vector CF203 (a pPZP212 derivative (Hajdukiewicz et al., 1994) containing the CaMV 35S-promoter, GFP5(S65T) gene and an rbcS terminator (kindly provided by C. Fankhauser, Lausanne)). Affinity mutants were designed from wild-type YbeJ ($K_d \approx 600$ nM) carrying different substitutions in position 179: A179R ($K_d \approx 10$ µM), A179V ($K_d \approx 100$ µM), and A179W ($K_d \approx 1$ mM) (Okumoto et al., 2005) and additional intermediate affinities that were generated in this work: A179Q ($K_d = 40 \pm 0{,}87$ µM; mean ± s. e. m. $n = 9$), A179Y ($K_d = 256 \pm 4{,}63$ µM; mean ± s. e. m. $n = 9$) and A179N ($K_d = 514 \pm 8{,}92$ µM; mean ± s. e. m. $n = 9$). Fluorescent indicator proteins for glutamate (FLIPE) sensors were named FLIPE-x^{display} or FLIPE-x^{cyt} depending on their expression at the surface (display) or in the cytosol (cyt), respectively. The resulting plasmids were called FLIPE-600n^{display}; FLIPE-10µ^{display}; FLIPE-40µ^{display}; FLIPE-100µ^{display}; FLIPE-250µ^{display}; FLIPE-500µ^{display}; FLIPE-1m^{display}; FLIPE-600n^{cyt} and FLIPE-10µ^{cyt}. Additionally, a FLIPE-600n^{display}-based construct lacking the C-terminal PDGFR transmembrane domain was generated (FLIPE-600n^{apo}) for apoplasmic targeting.

Agrobacterium tumefaciens GV3101 was transformed with the binary vectors and *Arabidopsis thaliana rdr6-11* silencing mutants were transformed by floral dipping. Seeds were surface-sterilized with 70% ethanol for 5 min followed by 30% sodium hypochloride for 10 min and rinsed with sterile, deionized water. Transformants were selected on half-strength Murashige and Skoog (MS) basal salt mixture including MES buffer (Duchefa Biochemies; cat No. M0254.0050) supplemented with 1% plant agar (pH 5.7) (Sigma, cat. no. 9002-18-0) and 1% sucrose. Seedlings were grown vertically under long-day light conditions (16 h light, 8 h dark) at a light intensity of about 100 µmol/m^2 sec for 3 days. To identify plant expressing the sensor, seedlings were preliminarily screened for GFP fluorescence (bandpass excitation filter at λ_{ex} = 470/40 nm, bandpass emission filter at λ_{em} = 525/50 nm, with a beam splitter at λ_{em} = 495 nm) using a fluorescence stereo zoom microscope ZEISS Axio Zoom.V16, which can detect ECFP and Venus fluorescence. Plant transformation with FLIPE sensors was carried out independently at least three times and yielded comparable results.

In vitro characterization of FLIPE affinity variants.

Affinity mutants carrying the substitution A179Q, A179Y and A179N were created by site-directed mutagenesis, and cloned into pRSET vector for protein expression in *E. coli*, adding an N-terminal His-6-tag to the constructs. Sequences were verified by sequencing. pRSET-FLIPE constructs were transferred to *E. coli* BL21(DE3) Gold (Stratagene) by chemical transformation. Colonies were inoculated in LB-media containing carbenicillin (Sigma Aldrich; cat No. 4800-94-6), 0.2% lactose (Merck; cat No. 7660.0250) and 0.05% glucose (Sigma Aldrich; cat No. 14431-43-7) and expressed for 2 h at 37 °C, 220 rpm shaking and then 48 h at 20 °C in darkness. Cells were harvested by centrifugation for 30 minutes at 4 °C, 13,000 x *g.* Sediments were resuspended in 20 mM sodium phosphate buffer (pH 7.0) containing protease inhibitors and lysed by sonication [Branson Sonifier cell disruptor B15; 10 cycles x (15s ON/OFF); 60% amplitude; 90% duty cycle], after which the lysate was centrifuged for 1 h at 4 °C, 13,000 x *g*. Supernatants were purified by histidine-affinity-chromatography. His-6-tagged proteins were eluted from the beads by using imidazole (AppliChem; cat No. A1073,0500; UN3263). Ligand titration curves were performed by using a

microplate reader TECAN™ Spark®. ECFP fluorescence was acquired at λ_{ex} = 430/10 nm and λ_{em} = 470/10 nm, respectively. Venus fluorescence was recorded with a bandpass excitation filter at λ_{ex} = 500/10 nm and a bandpass emission filter at λ_{em} = 530/10 nm. Intensity scans were performed at λ_{ex} = 430/10 nm and λ_{em} = 460-600/10 nm. All analyses were done using 20 mM sodium phosphate buffer, pH 7.0. The K_d of each FLIPE variant was determined by fitting to a single site binding isotherm as described previously (Okumoto et al., 2005). Affinities were calculated from at least three independent protein extracts.

Plant growth

Transgenic *Arabidopsis* lines stably expressing display, cytosolic or apoplasmic FLIPE constructs were grown in soil Floradur® (Floragard Vertriebs-GmbH products, Oldenburg, Germany) in individual 2.5-inch pots. Pots were arrayed in a 4 x 8 grid in standard greenhouse flats (Hermann Meyer KG products, Germany) and transferred to growth chambers with short day (8 h light, 16 h dark) or long day (16 h light, 8 h dark) conditions at 21°C and 50-70% RH. Plants were watered as needed, depending on growth stage. To determine rosette sizes, plants were imaged every week during 5 weeks until flowering. Size classification was carried out on 6-7-week-old plants grown under long day conditions. Images of the flowers from each transformant were acquired using a ZEISS Axio Zoom.V16 equipped with a ZEISS Axiocam 305 color camera. Image analysis to determine vegetative area and flower anatomy was performed using FIJI. Experiments were repeated four independent times, yielding comparable results.

Subcellular localization of FLIPE sensors

Images from FLIPE seedlings were collected on ZEISS laser scanning microscope (LSM) 880 equipped with Airyscan detector capable of fast acquisition mode. A C-Apochromat 40x/1.2 NA W Korr FCS M27 1 objective was used with water immersion. Sampling was performed in fast or super resolution mode, and scan speed was set to a pixel dwell time of 0.51 milliseconds. The pinhole was set to 2,24 airy units and line averaging was set to 8 or 16. Signal excitation for YFP and CFP was at λ_{ex} = 514 nm and λ_{ex} = 405 nm Argon laser, respectively, with emission detection at λ_{em} = 519-620 nm and λ_{em} = 474-492 nm, respectively, transmitted light images were collected with a PMT. Additional experiments were performed to validate the localization of the FLIPE^{display} sensor facing the apoplasm.

Subcellular localization assays were adapted from (Martinière et al., 2018) and repeated twice, yielding comparable results. Transient expression of the sensors was performed in leaves of 3-4-week-old *Nicotiana benthamiana* plants infiltrated with *Agrobacterium tumefaciens* strain GV3101 carrying constructs for FLIPE-1m^{display} and FLIPE-600n^{cyt}, as described below. In brief, 3 days past infiltration, protoplasts were obtained by digesting transformed leaves with 1.2% cellulose Onozuka R10 (Duchefa; cat No. C8001), 0.4% macerozyme R10 (Duchefa; cat No. M8002) in 0.4 M mannitol and MES 20 mM (pH 6.5) for 6-8 h at room temperature in the dark by shaking at 1x *g*. Protoplasts were pelleted at 100 x *g* and rinsed with fresh buffer. Preincubation with 50 µM cycloheximide (CHX, Sigma Aldrich; cat No. 66-81-9) for 30 min was followed by digestion with proteinase K at 50 µg/mL and 50 µM CHX. Slides with protoplasts were imaged under a confocal microscope for at least 20 min. Venus fluorescence intensity was quantified using FIJI (Schindelin et al., 2012).

Glutamate supplementation of FLIPE seedlings

Glutamate supplementation experiments were performed by measuring the growth of seedlings transformed with FLIPE constructs on square petri dishes with half-strength MS agar medium supplemented with 1% sucrose (Sigma Aldrich; cat No. 57-50-1) (as described above) covered with a layer of nylon mesh (Sefar Nitex 03-15/10). Three days after germination, seedlings on the mesh were transferred to a new half-strength MS agar medium supplemented with 1% sucrose containing

0 µM, 25 µM, 100 µM, 250 µM or 1 mM L-glutamic acid monosodium salt monohydrate (Sigma Aldrich, cat No. 6106-04-3). Plants were analyzed in single blinded-experiments. After transfer, plates were rotated 90° and plant were grown for 7 days under long day conditions (16 h light, 8 h dark). Seedlings were photographed daily during glutamate treatment and roots were measured using FIJI. Experiments were repeated three independent times and yielded comparable results.

Root tip (mPS)-PI staining

Modified pseudo-Schiff propidium iodide (mPS-PI) staining was performed as described by (Truernit et al., 2008), on root tips 5 days after germination. Samples were fixed in fixative solution [50% methanol (Sigma Aldrich, cat No. 67-56-1) and 10% acetic acid (Sigma Aldrich, cat No. 64-19-7)] at 4 °C overnight. Root tips were washed with water and incubated in 1% periodic acid at room temperature for 40 min. Then, tissues were rinsed and incubated in Schiff's reagent (Sigma Aldrich, cat No. 3952016) with propidium iodide (100 mM sodium metabisulphite and 0.15 N HCl; propidium iodide to a final concentration of 100 µg/mL freshly added) until samples were visibly stained. Roots were transferred to chloral hydrate solution [70% chloral hydrate (Sigma Aldrich, cat No. 302-17-0), 10% glycerol (Sigma Aldrich, cat No. 56-81-5)] and slides were prepared for microscope analysis adding drops of chloral hydrate solution and left covered overnight. The samples were examined with a 40x water immersion objective. Samples stained with propidium iodide were excited with a 561 nm argon laser with emission detection at 566-718 nm.

FRET imaging

FRET imaging was carried out as described previously (Chaudhuri et al., 2011). In brief, 7-days-old seedlings grown on hydroponic media were mounted on coverslips (24×50 mm No. 1½, VWR) using medical adhesive (Stock No. 7730, Hollister) to restrict movement (Deuschle et al., 2006). Chambers used for screening were made with plastic clay (Sculpey, www.sculpey.com) and were variable in size and volume (1–2 mL). For qualitative analyses, the clay chamber was filled with hydroponic medium, perfusion tubing was mounted, and roots were perfused at 3 mL · min^{-1}. Ratio imaging was performed on an inverted fluorescence microscope (DM IRE2, Leica) with a QuantEM digital camera (Roper) and a ×20 oil objective (HC PL APO ×20/0.7IMM CORR, Leica, Germany). Dual emission intensities were recorded simultaneously using a DualView with a dual CFP/YFP-ET filter set [high transmission modified Magnetron sputter-coated filter sets ET470/24m (470 indicates the emission wavelength, /24 indicates bandwidth); ET535/3, Chroma, USA] and Slidebook software (Intelligent Imaging Innovations Inc., USA]. Data was analyzed with ImageJ (rsb.info.nih.gov/ij/).

References

Ast C, Foret J, Oltrogge LM, Michele RD, Kleist TJ, Ho C-H, Frommer WB. 2017. Ratiometric Matryoshka biosensors from a nested cassette of green- and orange-emitting fluorescent proteins. *Nat Comm* **8**:431. doi:10.1038/s41467-017-00400-2

Barnett LM, Hughes TE, Drobizhev M. 2017. Deciphering the molecular mechanism responsible for GCaMP6m's Ca^{2+}-dependent change in fluorescence. *PLoS One* **12**:e0170934. doi:10.1371/journal.pone.0170934

Chaudhuri B, Hörmann F, Frommer WB. 2011. Dynamic imaging of glucose flux impedance using FRET sensors in wild-type Arabidopsis plants. *J Exp Bot* **62**:2411–7. doi:10.1093/jxb/erq444

Denyer T, Ma X, Klesen S, Scacchi E, Nieselt K, Timmermans MCP. 2019. Spatiotemporal developmental trajectories in the Arabidopsis root revealed using high-throughput single-cell RNA sequencing. *Dev Cell* **48**:840-852.e5. doi:10.1016/j.devcel.2019.02.022

Deuschle K, Chaudhuri B, Okumoto S, Lager I, Lalonde S, Frommer WB. 2006. Rapid metabolism of glucose detected with FRET glucose nanosensors in epidermal cells and intact roots of Arabidopsis RNA-silencing mutants. *Plant Cell* **18**:2314–25.

Deuschle K, Okumoto S, Fehr M, Looger LL, Kozhukh L, Frommer WB. 2005. Construction and optimization of a family of genetically encoded metabolite sensors by semirational protein engineering. *Protein Sci* **14**:2304–14. doi:10.1110/ps.051508105

Forde BG, Lea PJ. 2007. Glutamate in plants: metabolism, regulation, and signalling. *J Exp Bot* **58**:2339–2358. doi:10.1093/jxb/erm121

Frommer WB, Davidson MW, Campbell RE. 2009. Genetically encoded biosensors based on engineered fluorescent proteins. *Chem Soc Rev* **38**:2833–41. doi:10.1039/b907749a

Hajdukiewicz P, Svab Z, Maliga P. 1994. The small, versatile pPZP family of Agrobacterium binary vectors for plant transformation. *Plant Mol Biol* **25**:989–994.

Hirner A, Ladwig F, Stransky H, Okumoto S, Keinath M, Harms A, Frommer WB, Koch W. 2006. Arabidopsis LHT1 is a high-affinity transporter for cellular amino acid uptake in both root epidermis and leaf mesophyll. *Plant Cell* **18**:1931–46. doi:10.1105/tpc.106.041012

Huang F, Luo J, Ning T, Cao W, Jin X, Zhao H, Wang Y, Han S. 2017. Cytosolic and nucleosolic calcium signaling in response to osmotic and salt stresses are independent of each other in roots of Arabidopsis seedlings. *Front Plant Sci* **8**. doi:10.3389/fpls.2017.01648

Kiss JZ, Wright JB, Caspar T. 1996. Gravitropism in roots of intermediate-starch mutants of Arabidopsis. *Physiol Plant* **97**:237–244. doi:10.1034/j.1399-3054.1996.970205.x

Li J, Zhu S, Song X, Shen Y, Chen H, Yu J, Yi K, Liu Y, Karplus VJ, Wu P, Deng XW. 2006. A rice glutamate receptor-like gene is critical for the division and survival of individual cells in the root apical meristem. *Plant Cell* **18**:340–349. doi:10.1105/tpc.105.037713

Mahmoud S, Gharagozloo M, Simard C, Gris D. 2019. Astrocytes maintain glutamate homeostasis in the CNS by controlling the balance between glutamate uptake and release. *Cells* **8**. doi:10.3390/cells8020184

Martinière A, Gibrat R, Sentenac H, Dumont X, Gaillard I, Paris N. 2018. Uncovering pH at both sides of the root plasma membrane interface using noninvasive imaging. *Proc Natl Acad Sci USA* **115**:6488–6493. doi:10.1073/pnas.1721769115

Marvin JS, Borghuis BG, Tian L, Cichon J, Harnett MT, Akerboom J, Gordus A, Renninger SL, Chen T-W, Bargmann CI, Orger MB, Schreiter ER, Demb JB, Gan W-B, Hires SA, Looger LL. 2013. An optimized fluorescent probe for visualizing glutamate neurotransmission. *Nat Methods* **10**:162–170. doi:10.1038/nmeth.2333

Mousavi SAR, Chauvin A, Pascaud F, Kellenberger S, Farmer EE. 2013. GLUTAMATE RECEPTOR-LIKE genes mediate leaf-to-leaf wound signalling. *Nature* **500**:422–426. doi:10.1038/nature12478

Nguyen CT, Kurenda A, Stolz S, Chételat A, Farmer EE. 2018. Identification of cell populations necessary for leaf-to-leaf electrical signaling in a wounded plant. *Proc Natl Acad Sci USA* **115**:10178–10183. doi:10.1073/pnas.1807049115

Okumoto S, Jones A, Frommer WB. 2012. Quantitative imaging with fluorescent biosensors. *Annu Rev Plant Biol* **63**:663–706. doi:10.1146/annurev-arplant-042110-103745

Okumoto S, Looger LL, Micheva KD, Reimer RJ, Smith SJ, Frommer WB. 2005. Detection of glutamate release from neurons by genetically encoded surface-displayed FRET nanosensors. *Proc Natl Acad Sci USA* **102**:8740–5. doi:10.1073/pnas.0503274102

Okumoto S, Takanaga H, Frommer WB. 2008. Quantitative imaging for discovery and assembly of the metabo-regulome. *New Phytol* **180**:271–95. doi:10.1111/j.1469-8137.2008.02611.x

Sabetta W, Vandelle E, Locato V, Costa A, Cimini S, Bittencourt Moura A, Luoni L, Graf A, Viggiano L, De Gara L, Bellin D, Blanco E, Pinto MC. 2019. Genetic buffering of cyclic AMP in *Arabidopsis thaliana* compromises the plant immune response triggered by an avirulent strain of *Pseudomonas syringae* pv. *tomato*. *Plant J* **98**:590–606. doi:10.1111/tpj.14275

Schindelin J, Arganda-Carreras I, Frise E, Kaynig V, Longair M, Pietzsch T, Preibisch S, Rueden C, Saalfeld S, Schmid B, Tinevez JY, White DJ, Hartenstein V, Eliceiri K, Tomancak P, Cardona A. 2012. Fiji: an open-source platform for biological-image analysis. *Nat Methods* **9**:676–82. doi:10.1038/nmeth.2019

Singh SK, Chang I-F. 2017. Pharmacological studies with specific agonist and antagonist of animal iGluR on root growth in *Arabidopsis thaliana*. GABA And Glutamate - New Developments In Neurotransmission Research, IntechOpen. p. DOI: 10.5772/intechopen.72121.

Singh SK, Chien C-T, Chang I-F. 2016. The Arabidopsis glutamate receptor-like gene GLR3.6 controls root development by repressing the Kip-related protein gene KRP4. *J Exp Bot* **67**:1853–1869. doi:10.1093/jxb/erv576

Toyota M, Spencer D, Sawai-Toyota S, Jiaqi W, Zhang T, Koo AJ, Howe GA, Gilroy S. 2018. Glutamate triggers long-distance, calcium-based plant defense signaling. *Science* **361**:1112–1115. doi:10.1126/science.aat7744

Truernit E, Bauby H, Dubreucq B, Grandjean O, Runions J, Barthelemy J, Palauqui JC. 2008. High-resolution whole-mount imaging of three-dimensional tissue organization and gene expression enables the study of phloem development and structure in Arabidopsis. *Plant Cell* **20**:1494–503. doi:10.1105/tpc.107.056069

Vincill ED, Clarin AE, Molenda JN, Spalding EP. 2013. Interacting glutamate receptor-like proteins in phloem regulate lateral root initiation in Arabidopsis. *Plant Cell* **25**:1304–13. doi:10.1105/tpc.113.110668

Walch-Liu P, Liu L-H, Remans T, Tester M, Forde BG. 2006. Evidence that L-glutamate can act as an exogenous signal to modulate root growth and branching in *Arabidopsis thaliana*. *Plant Cell Physiol* **47**:1045–1057. doi:10.1093/pcp/pcj075

Wang X, Yang G, Shi M, Hao D, Wei Q, Wang Z, Fu S, Su Y, Xia J. 2019. Disruption of an amino acid transporter LHT1 leads to growth inhibition and low yields in rice. *BMC Plant Biology* **19**:268. doi:10.1186/s12870-019-1885-9

Willis RC, Furlong CE. 1975. Purification and properties of a periplasmic glutamate-aspartate binding protein from *Escherichia coli* K12 strain W3092. *J Biol Chem* **250**:2574–2580.

AUTHOR CONTRIBUTIONS

Conceptualization: VCR, MW, SO, WBF, TK; Methodology: NG, SO, VCR, TK, TD, MT, MW; Investigation, NG, SO, VCR, TK, MM, MW; Writing, VCR, TK, WBF; MW Supervision: WBF, TK, MW.

ACKNOWLEDGEMENTS

We would like to thank Rüdiger Simon's group for assistance with PI staining of roots and the center for advanced imaging (CAi) at HHU for help with image acquisition. This research was funded by grants from Deutsche Forschungsgemeinschaft (DFG, German Research Foundation) under Germany´s Excellence Strategy – EXC-2048/1 – project ID 390686111 and Deutsche Forschungsgemeinschaft (DFG, German Research Foundation) – Project-ID 267205415 – SFB 1208 – Project-ID 267205415 – as well as the Alexander von Humboldt Foundation to WBF.

Tables and Figures

Tables

Table 1. Effect of FLIPE sensor variants on the lethality in Arabidopsis grown under long day conditions.

sensor	# of plants transferred in soil	# of plants that survived after			% survival*	% lethal*
		week 2	week 4	week 6		
FLIPE-600n^{display}	55	12	3	0	0	100
FLIPE-10µ^{display}	51	15	7	0	0	100
FLIPE-100µ^{display}	65	19	11	6	9	90
FLIPE-1m^{display}	73	34	30	23	32	68
FLIPE-600n^{cyt}	107	106	106	106	99	1
FLIPE-10µ^{cyt}	109	108	108	108	99	1
control *(rdr6-11)*	103	102	102	102	99	1

* after Week 6

Figures

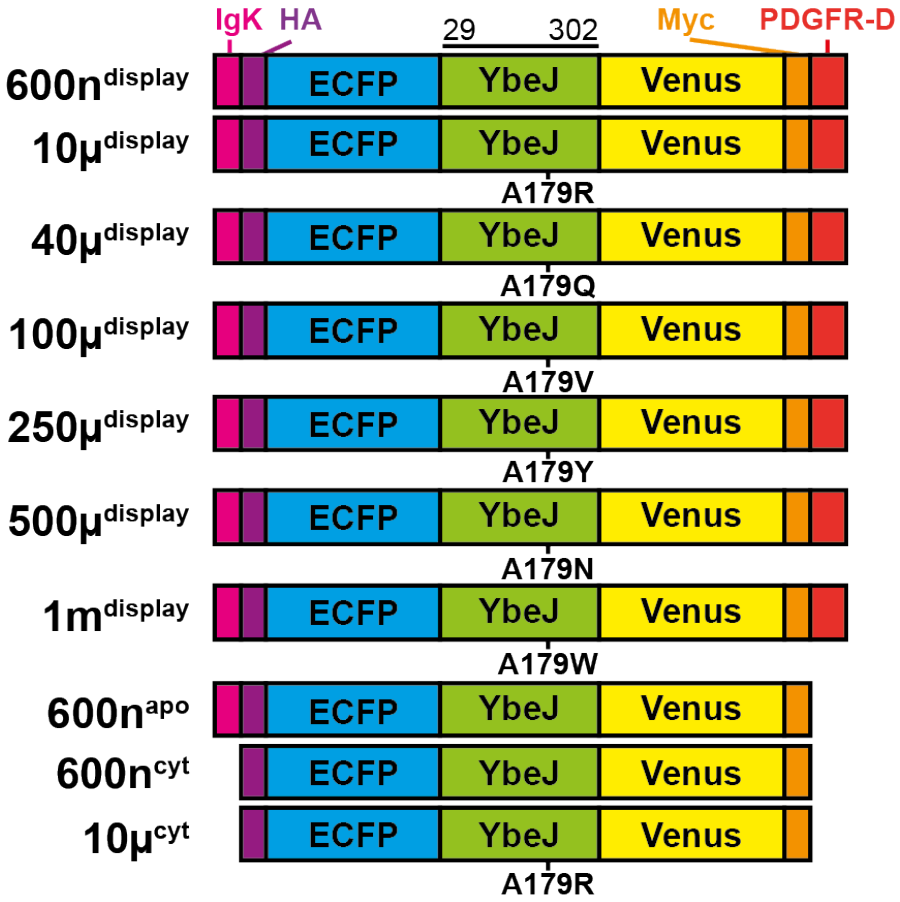

Figure 1. Schematic representation of FLIPE sensor variants. FLIPE^{display} and FLIPE^{cyt} cassette containing the fluorescent proteins ECFP and Venus flanking amino acids 29-302 of the periplasmic glutamate binding protein YbeJ from *E. coli*. Display sensor constructs contain sequences for an IgK ER targeting sequence, an HA tag at the 5'-end, and a c-Myc tag followed by the transmembrane spanning domain of the human PDGF receptor. Amino acid changes in YbeJ at position 179 yielding different glutamate binding affinities are highlighted. The sequence of the 600n^{apo} construct is equal to the 600n^{display} construct but missing PDGFR domain.

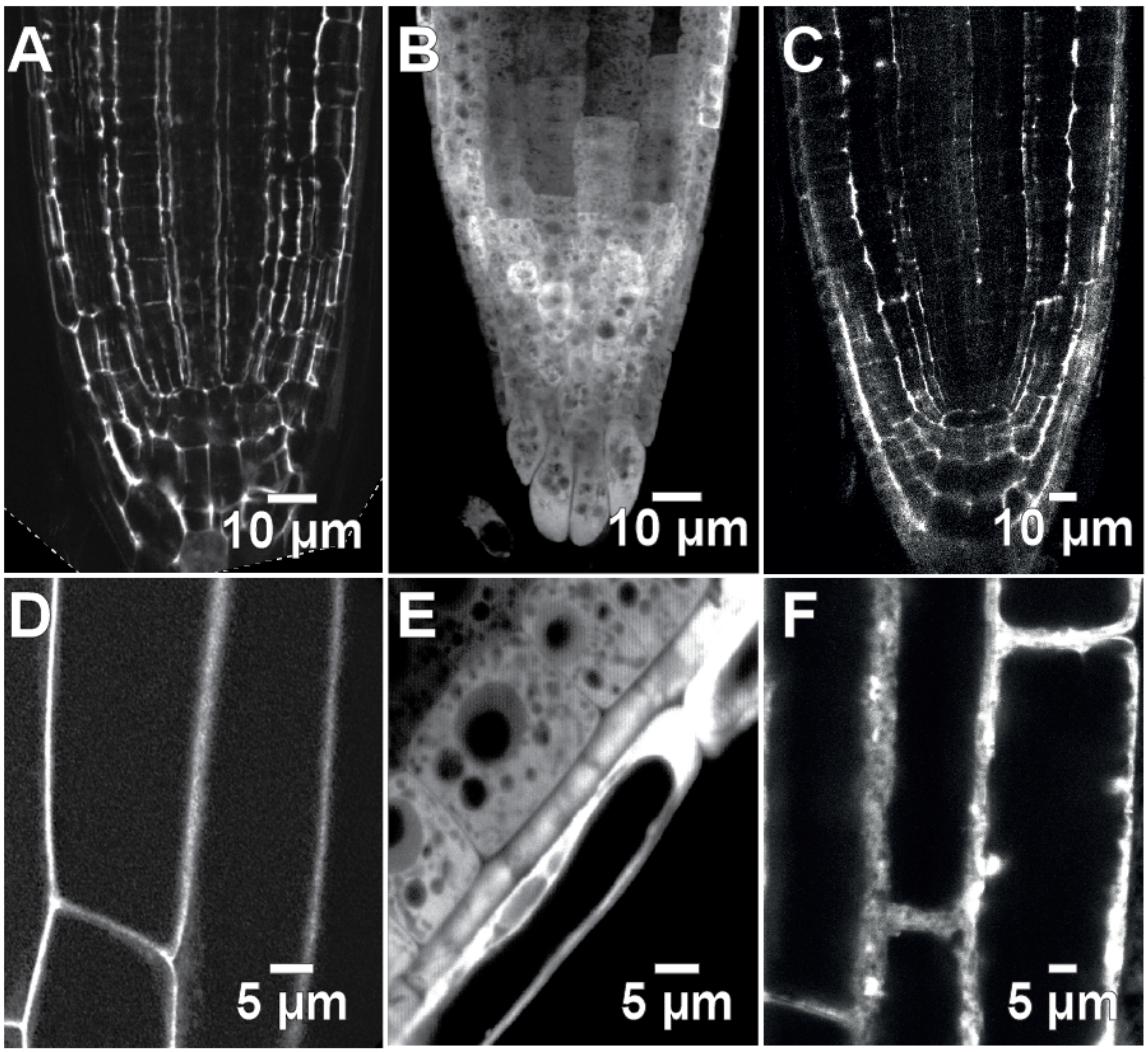

Figure 2. Subcellular localization of FLIPE sensors in the root tip. Representative confocal images in differentiating root tip cells of 3-5-day-old plant expressing FLIPE-600n^{display} (A), FLIPE-600n^{cyt} (B) and FLIPE-600n^{apo} (C) sensors. Higher magnification of root tip regions depicts a localization of FLIPE-600n^{display} in the plasma membrane (D) while FLIPE-600n^{cyt} is localized throughout the cytosol (E) and FLIPE-600n^{apo} to the apoplasmic space (F).

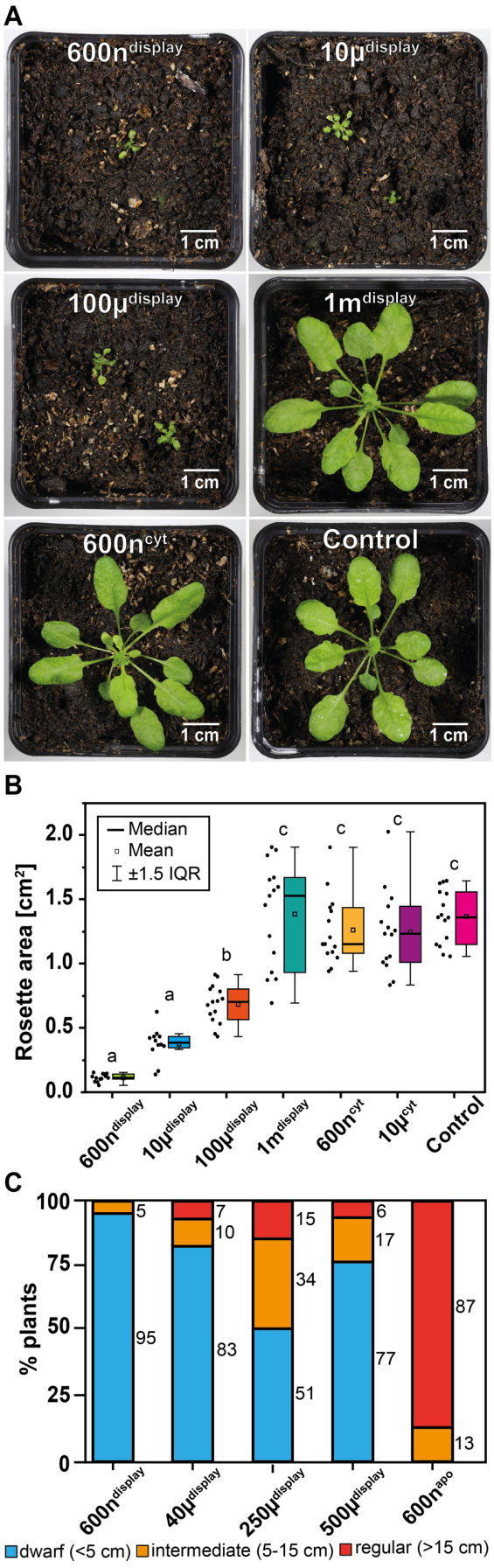

Figure 3. Phenotypic characterization of FLIPE sensor-expressing plants. (A) Representative phenotypes of 6-week-old soil-grown plants expressing FLIPE sensor affinity variants and the corresponding *rdr6-11* control. (B) Quantification of rosette areas of 3-weeks-old soil-grown plants expressing different FLIPE sensors ($n \geq 12$ plants per genotype from 4 independent biological replicates). Compared to *rdr6-11* control plants, FLIPE-600n^{display}, FLIPE-10µ^{display} and FLIPE-100µ^{display} plants showed significantly smaller rosettes, respectively, while the rosette sizes of cytosolic sensor variants and of the low-affinity FLIPE-1m^{display} line were not significantly different from the control (Tukey test, $P < 0.001$, letters indicate if samples are statistically indifferent (same letters) or different (different letters) from one another). (C) Phenotypic characterization into 'dwarf', 'intermediate' and 'regular' growth of several FLIPE^{display} and a FLIPE^{apo} version ($n \geq 21$).

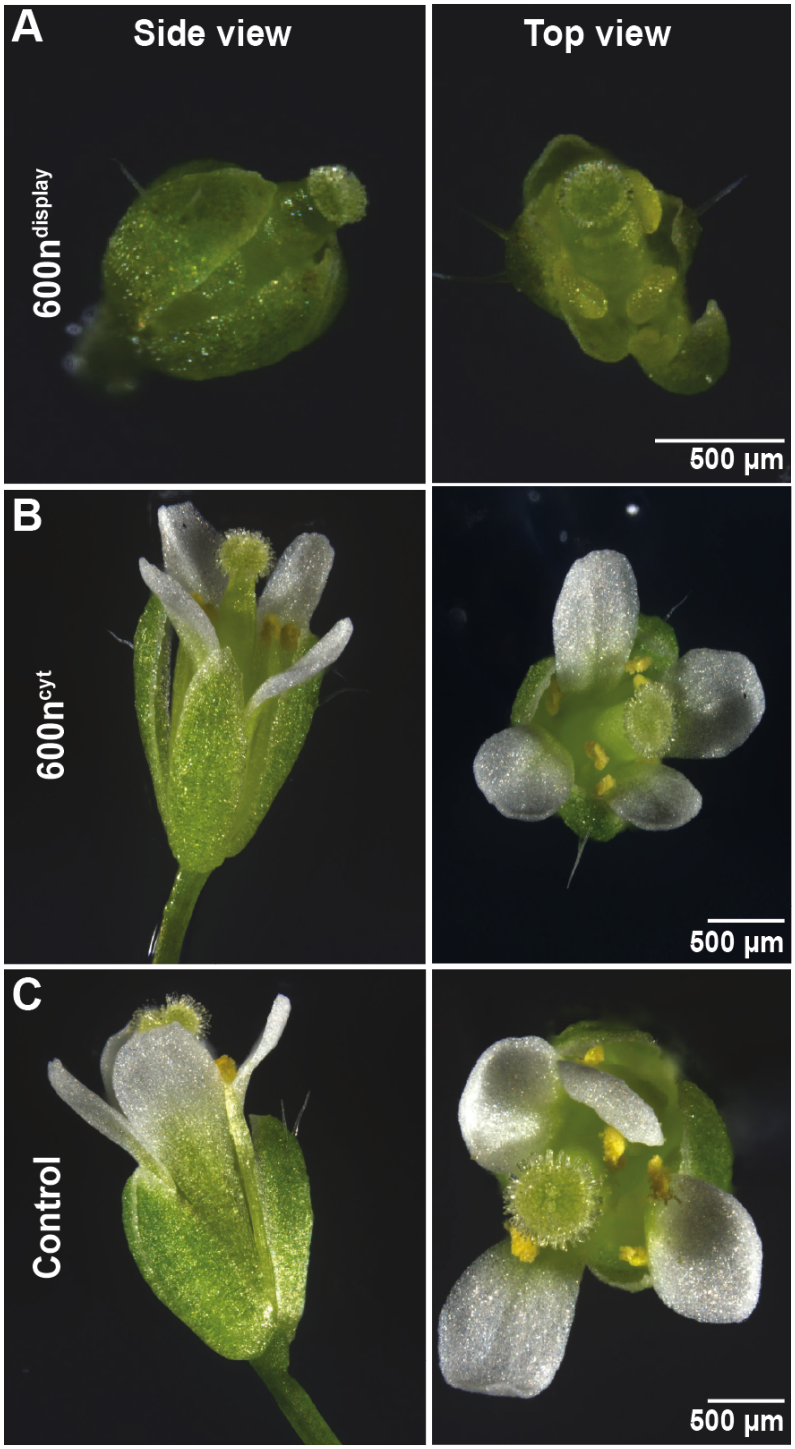

Figure 4. Phenotype of flowers from Arabidopsis control plants and lines expressing FLIPE^{display} or FLIPE^{cyt} constructs. Representative flowers form FLIPE-600n^{display} (A), FLIPE-600n^{cyt} (B) or control (*rdr6-11*) plants (C).

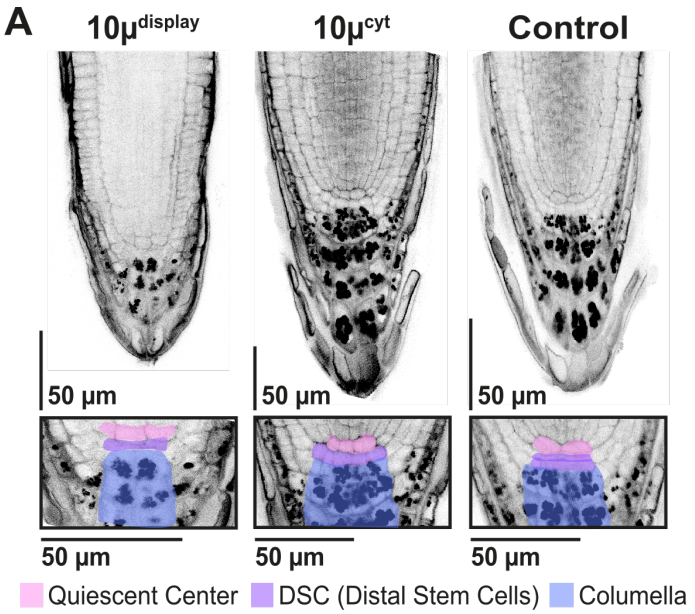

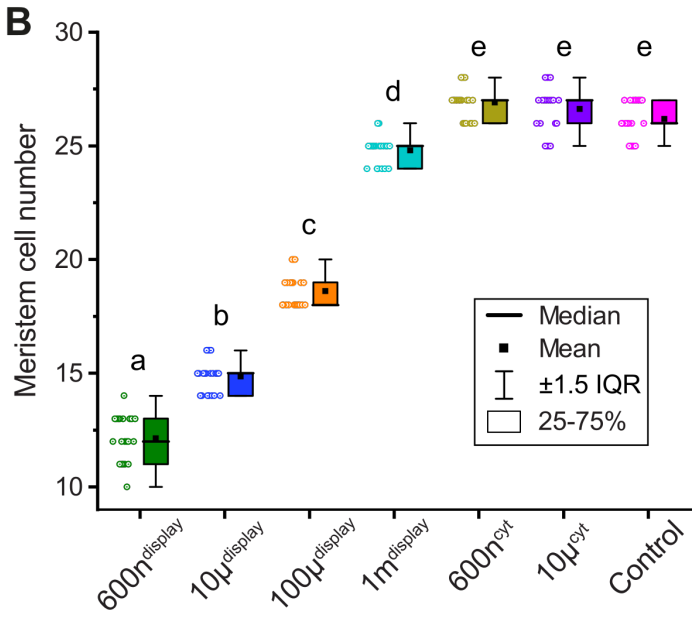

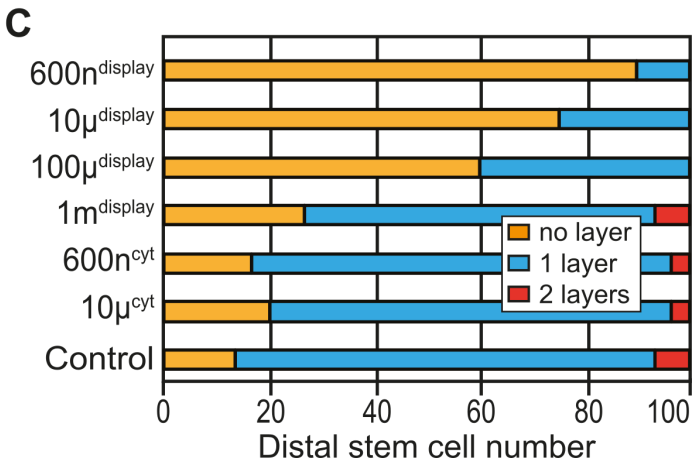

Figure 5. Effect of FLIPE sensor expression on the root apical meristem and the distal stem cell niche. (A) Representative root tips of plants expressing display and cytosolic FLIPE variants grown on half-strength MS medium for 3-5 days after germination (top panel) and zoom-in of respective proximal meristems (lower panel). The color code highlights the Quiescent Center (pink), Distal Stem Cells (purple) and Columella cells (blue). (B) Comparison of the size of the meristematic zone of the different FLIPE sensor lines, displaying the number of meristematic cells between QC and root elongation zone. Meristem cell numbers were statistically different in FLIPE-600n^{display}, FLIPE-10μ^{display}, FLIPE-100μ^{display}, compared to control (*rdr6-11*; Tukey test $P < 0.001$, letters indicate if samples are statistically indifferent (same letters) or different (different letters) from one another). Data was acquired from 6 independent biological replicates, n = 17-21. (C) Percentage of roots with no undifferentiated distal stem cell (DSC) layers (yellow bar), one cell layer (blue bar) or two cell layers (red bar); experiment performed 3 independent times; n = 22.

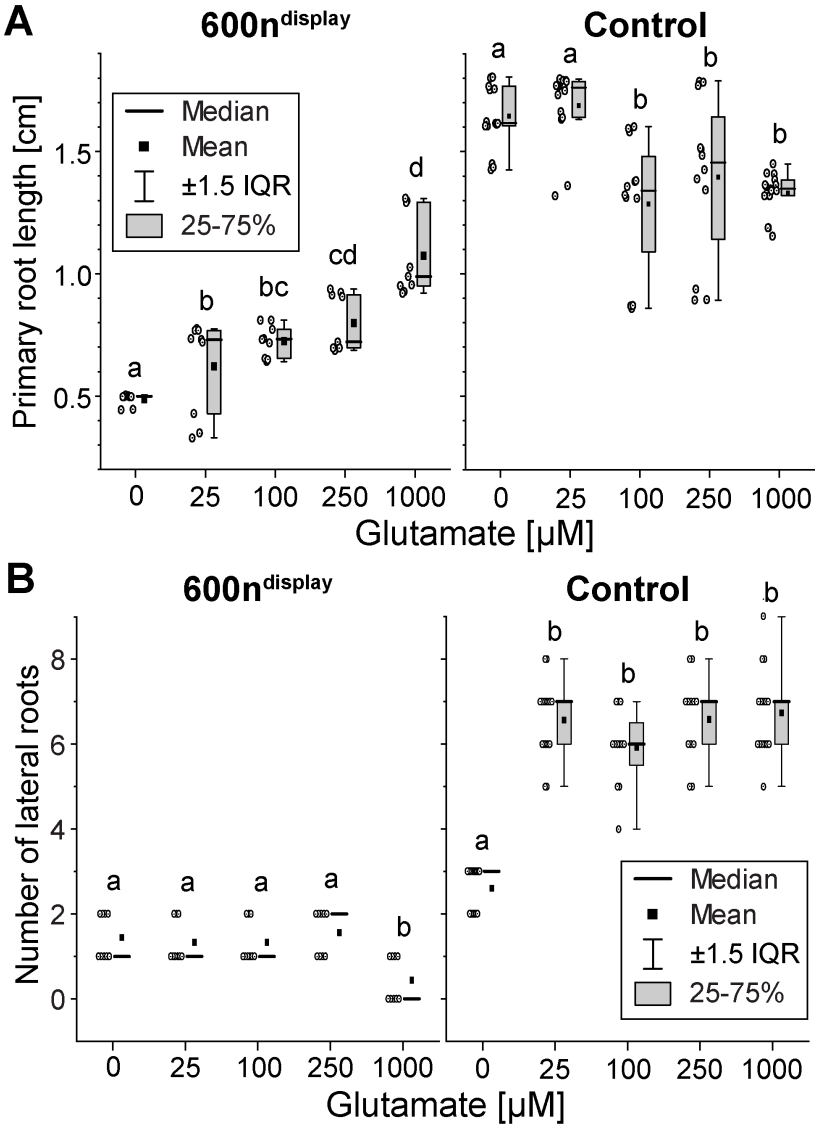

Figure 6. Supplementation with glutamate of FLIPE-600n^{display}-expressing plants. (A) Primary root growth of vertically grown FLIPE-600n^{display} (left) or *rdr6-11* control (right) Arabidopsis seedlings 5 days after transfer to half-strength MS agar medium plates with increasing concentrations of glutamate. While roots of control plants did not significantly grow at [glu] ≥ 100µM, roots of FLIPE-600n^{display} lines were still growing at [glu] of 1mM. (B) Number of lateral roots of FLIPE-600n^{display} (left) or *rdr6-11* control plants (right). Letters indicate if samples are statistically indifferent (same letters) or different (different letters) from one another. The experiment was performed three independent times with ≥ 3 roots per treatment.